Nuclear Engineering and Technology 54 (2022) 1495–1507

Contents lists available at ScienceDirect

Nuclear Engineering and Technology

journal homepage: www.elsevier.com/locate/net

Original Article

Partition method of wall friction and interfacial drag force model for horizontal two-phase flows

Takashi Hibiki [a, **], Jae Jun Jeong [b, *]

[a] Department of Mechanical Engineering, City University of Hong Kong, 83 Tat Chee Avenue, Kowloon Tong, Hong Kong, China
[b] School of Mechanical Engineering, Pusan National University, Geumjeong-gu, Busan, 46241, Republic of Korea

ARTICLE INFO

Article history:
Received 22 June 2021
Received in revised form
21 September 2021
Accepted 10 October 2021
Available online 14 October 2021

Keywords:
Two-fluid model
Thermal-hydraulic system code
Wall friction partition
Horizontal flow
Interfacial drag force

ABSTRACT

The improvement of thermal-hydraulic analysis techniques is essential to ensure the safety and reliability of nuclear power plants. The one-dimensional two-fluid model has been adopted in state-of-the-art thermal-hydraulic system codes. Current constitutive equations used in the system codes reach a mature level. Some exceptions are the partition method of wall friction in the momentum equation of the two-fluid model and the interfacial drag force model for a horizontal two-phase flow. This study is focused on deriving the partition method of wall friction in the momentum equation of the two-fluid model and modeling the interfacial drag force model for a horizontal bubbly flow. The one-dimensional momentum equation in the two-fluid model is derived from the local momentum equation. The derived one-dimensional momentum equation demonstrates that total wall friction should be apportioned to gas and liquid phases based on the phasic volume fraction, which is the same as that used in the SPACE code. The constitutive equations for the interfacial drag force are also identified. Based on the assessments, the Rassame-Hibiki correlation, Hibiki-Ishii correlation, Ishii-Zuber correlation, and Rassame-Hibiki correlation are recommended for computing the distribution parameter, interfacial area concentration, drag coefficient, and relative velocity covariance of a horizontal bubbly flow, respectively.

1. Introduction

The improvement of thermal-hydraulic analysis techniques is essential to ensure the safety and reliability of nuclear power plants [1]. A variety of numerical simulation codes are available depending on the size of the target control volume. System analysis codes, porous media codes, and subchannel analysis codes have been used for nuclear system analysis, steam generator simulation, and core analysis, respectively. Computational fluid dynamics codes based on the two-fluid model [2] and large-eddy simulations [3] are also being developed for detailed local flow simulations. Experimental techniques to measure local two-phase flow parameters are underway to validate the codes [4,5]. Constitutive equations have been developed based on a physical understanding of the relevant phenomena and experimental data. The developed constitutive equations are being implemented in simulation codes to improve prediction accuracy.

The one-dimensional two-field two-fluid model has been adopted in state-of-the-art nuclear thermal-hydraulic system analysis codes, such as RELAP5/MOD3 [6], RELAP5-3D [7], TRAC-PF1 [7], TRACE V5 [8], CATHARE 2 [9], and MARS [10]. The one-dimensional three-field model has also been implemented in new system codes, such as CATHARE 3 [11] and SPACE [12]. Current constitutive equations used in the one-dimensional system analysis codes reach a mature level. Still, some exceptions are the partition method of wall friction in the momentum equation of the two-fluid model and the interfacial drag force model for a horizontal two-phase flow.

Lee et al. [13] pointed out that one-dimensional thermal-hydraulic system analysis codes adopted different partition methods of wall friction. They simulated horizontal air-water bubbly flows using RELAP5/MOD3 [6], TRACE V5 [8], and SPACE [12] codes to identify the effect of the partition method on the prediction of void fraction and slip ratio. The RELAP5 and SPACE codes computed the slip ratio nearly equal to unity, whereas the TRACE code computed the slip ratio higher than 1.1. Lee et al. attributed the unphysical slip ratio primarily to the improper partition method of wall friction adopted in the TRACE code. They also expected unphysical droplet

* Corresponding author.
** Corresponding author.
E-mail addresses: thibiki@cityu.edu (T. Hibiki), jjjeong@pusan.ac.kr (J.J. Jeong).

https://doi.org/10.1016/j.net.2021.10.014

behavior in horizontal mist flows computed based on the two-fluid model if the wall friction was not properly apportioned between gas and droplet phases. Since this might cause significant issues in a LOCA simulation of PWRs, Lee et al. strongly recommended revisiting the two-fluid model with a particular focus on the partition method of two-phase wall friction. They claimed that one solution to this issue was the phasic momentum equation based on the equation of a fluid particle motion adopted in the SPACE code [14].

Due to the importance of the partition method of wall friction in the momentum equation and interfacial drag force model for a horizontal two-phase flow, the current study is focused on deriving the partition method of wall friction in the momentum equation of the two-fluid model and modeling the interfacial drag force model for a horizontal bubbly flow. The current study also identifies necessary constitutive equations to calculate the interfacial drag force. The required constitutive equations include the equations for distribution parameter, interfacial area concentration, drag coefficient, and relative velocity covariance. The derived partition method of wall friction and modeled interfacial drag force are expected to improve the robustness and accuracy of nuclear thermal-hydraulic system analysis codes.

2. Brief review of partition method of wall friction and interfacial drag force

2.1. One-dimensional momentum equation

The one-dimensional momentum equation in the two-fluid model is expressed by Ref. [2]:

$$\frac{\partial\langle\alpha_k\rangle\rho_k\langle\langle v_k\rangle\rangle}{\partial t}+\frac{\partial}{\partial z}\langle\alpha_k\rangle\rho_k\langle\langle v_k\rangle\rangle^2=-\langle\alpha_k\rangle\frac{\partial p_k}{\partial z}-\langle\alpha_k\rangle\rho_k g_z+\langle\mathbf{M}_{ik}\rangle_z-\langle M_{wk}\rangle \tag{1}$$

where α, ρ, v, t, z, p, g, M_i, and M_w are the void fraction, density, velocity, time, axial coordinate, pressure, gravitational acceleration, generalized interfacial drag force, and wall friction, respectively. $\langle\rangle$ and $\langle\langle\rangle\rangle$ are the area-averaged and void fraction-weighted mean quantities, respectively. The subscript, k, indicates the phase (g for gas phase and f for liquid phase).

The generalized interfacial drag force includes the interfacial drag force, virtual mass force, etc. Under a steady-state fully-developed flow condition, the generalized interfacial drag force only considers the interfacial drag force, which is expressed by:

$$\langle\mathbf{M}_{ik}\rangle_z=(-1)^k C_i|\langle v_r\rangle|\langle v_r\rangle \tag{2}$$

where C_i and v_r are the overall drag coefficient and velocity difference between gas and liquid phases (or relative velocity), respectively.

Lee et al. [13] considered a steady-state fully-developed flow in a horizontal channel and obtained the gas momentum equation by simplifying Eq. (1) as:

$$-\langle\alpha_g\rangle\frac{\partial p_g}{\partial z}\simeq C_i|\langle v_r\rangle|\langle v_r\rangle+\langle M_{wg}\rangle \tag{3}$$

Equation (3) indicates that the accurate prediction of the void fraction depends on the precise formulation of the phasic wall friction and interfacial drag force. The effect of the phasic wall friction and interfacial drag force models on void fraction prediction is more pronounced for a horizontal dispersed flow where the buoyancy force is not exerted along the flow direction.

2.2. Partitioning of wall friction

The total two-phase wall friction, $M_{w2\phi}$, is partitioned into gas and liquid phases. Different codes utilize different partition methods as follows.

RELAP5/MOD3 [6].

$$\langle M_{wg}\rangle=\frac{\alpha_{gw}\lambda_g\rho_g\langle\langle v_g\rangle\rangle^2}{\alpha_{gw}\lambda_g\rho_g\langle\langle v_g\rangle\rangle^2+\alpha_{fw}\lambda_f\rho_f\langle\langle v_f\rangle\rangle^2}\langle M_{w2\phi}\rangle \tag{4}$$

$$\langle M_{wf}\rangle=\frac{\alpha_{fw}\lambda_f\rho_f\langle\langle v_f\rangle\rangle^2}{\alpha_{gw}\lambda_g\rho_g\langle\langle v_g\rangle\rangle^2+\alpha_{fw}\lambda_f\rho_f\langle\langle v_f\rangle\rangle^2}\langle M_{w2\phi}\rangle \tag{5}$$

where λ is the Darcy-Weisbach friction factor. In a bubbly flow regime, the wall void fraction, α_{gw}, and wall liquid fraction, α_{fw}, are assumed by:

$$\alpha_{gw}=\langle\alpha_g\rangle \text{ and } \alpha_{fw}=\langle\alpha_f\rangle \tag{6}$$

TRACE V5 [8].

$$\langle M_{wg}\rangle=0 \tag{7}$$

$$\langle M_{wf}\rangle=\langle M_{w2\phi}\rangle \tag{8}$$

SPACE [12].

$$\langle M_{wg}\rangle=\langle\alpha_g\rangle\langle M_{w2\phi}\rangle \tag{9}$$

$$\langle M_{wf}\rangle=\langle\alpha_f\rangle\langle M_{w2\phi}\rangle \tag{10}$$

The partition method is generalized as:

$$\langle M_{wg}\rangle=c_g\langle M_{w2\phi}\rangle \tag{11}$$

$$\langle M_{wf}\rangle=c_f\langle M_{w2\phi}\rangle \tag{12}$$

where c is the partition coefficient. In the TRACE code, $c_g=0$ and $c_f=1$, whereas $c_g=\langle\alpha_g\rangle$ and $c_f=\langle\alpha_f\rangle$ in the SPACE code.

Fig. 1 shows a sample calculation to compare the partition coefficient between the RELAP5 and the SPACE codes. The calculation conditions are the channel geometry of a circular channel with an inner diameter of 38.1 mm, horizontal channel orientation, steam-water system, pressure of 7.0 MPa, and fixed superficial liquid velocity. The sample calculation considers bubbly flow or finely-dispersed bubbly flow regimes. The void fraction for the horizontal flow is calculated by Rassame-Hibiki drift-flux correlation [15]. The solid black and broken red lines indicate the partition coefficients of the gas phase calculated by the RELAP5 code model, Eq. (4) and SPACE code model, Eq. (9), respectively. The partition coefficient of the gas phase in the TRACE code is zero, see Eq. (7). The broken red line also corresponds to the area-averaged void fraction because $c_g=\langle\alpha_g\rangle$ in the SPACE code model.

As shown in Fig. 1, when the void fraction is lower than 0.1, the partition coefficient of the gas phase calculated by the RELAP5 code model is less than 0.01, i.e., $c_g\simeq 0$ and $c_f\simeq 1$, which is close to the partition coefficient of the gas phase adopted in the TRACE code. When the void fraction increases, the partition coefficient of the gas phase approaches the void fraction, i.e., $c_g\simeq\langle\alpha_g\rangle$ and $c_f\simeq\langle\alpha_f\rangle$, corresponding to the partition coefficients adopted in the SPACE code model. Thus, the partition coefficient of the gas phase in the RELAP5 code model is in-between the partition coefficients of the gas phase in the TRACE and SPACE code models. However, under low-pressure conditions, the partition coefficient in the RELAP5 code

model is almost identical to that in the TRACE code model, $c_g \simeq 0$, due to gas density negligibly smaller than liquid density.

The effect of the partition coefficient model on the relative velocity between two phases is briefly discussed as follows. Substituting Eq. (11) into Eq. (3) yields:

$$-\langle\alpha_g\rangle\frac{\partial p_g}{\partial z} = C_i|\langle v_r\rangle|\langle v_r\rangle + c_g\langle M_{w2\phi}\rangle \tag{13}$$

For bubbly flow, the total two-phase frictional pressure drop is assumed by Ref. [13]:

$$\langle M_{w2\phi}\rangle \simeq -\frac{\partial p_g}{\partial z} > 0 \tag{14}$$

Substituting Eq. (14) into Eq. (13) yields:

$$\left(\langle\alpha_g\rangle - c_g\right)\left(-\frac{\partial p_g}{\partial z}\right) = C_i|\langle v_r\rangle|\langle v_r\rangle \tag{15}$$

Thus,

$$C_i|\langle v_r\rangle|\langle v_r\rangle = \begin{cases} \left(\langle\alpha_g\rangle - c_g\right)\left(-\frac{\partial p_g}{\partial z}\right) & \text{for RELAP5} \\ \langle\alpha_g\rangle\left(-\frac{\partial p_g}{\partial z}\right). > 0 & \text{for TRACE} \\ \sim 0 & \text{for SPACE} \end{cases} \tag{16}$$

Lee et al. [14] discussed that the SPACE code calculates nearly zero area-averaged relative velocity between two phases for a horizontal two-phase flow. However, the TRACE code calculates a positive area-averaged relative velocity for a horizontal two-phase flow, which means the gas phase travels faster than the liquid phase. Although the area-averaged relative velocity calculated by RELAP5 code depends on the sign of $\langle\alpha_g\rangle - c_g$, it is expected that the RELAP5 code may calculate a positive area-averaged relative velocity for a horizontal two-phase flow but with a slip ratio smaller than that of the TRACE code.

2.3. Interfacial drag force

Two methods are commonly used in calculating the interfacial drag force.

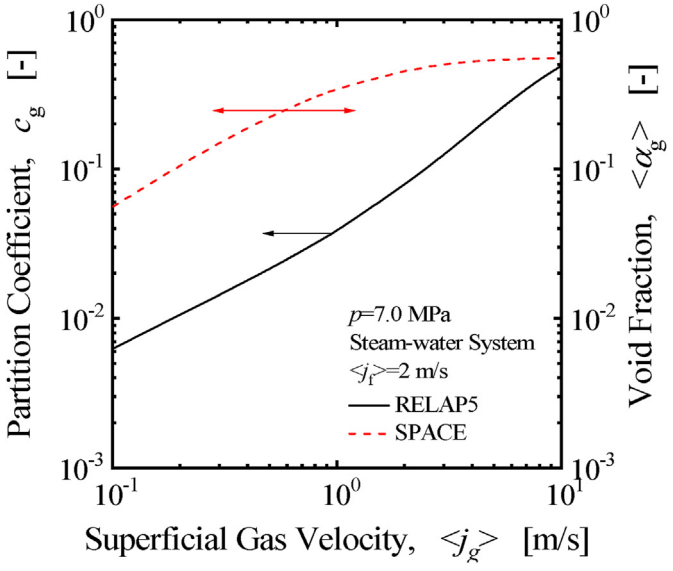

Fig. 1. Comparison of partition coefficient between RELAP5 and SPACE codes.

Drift velocity approach [16] is given as:

$$\langle M_{ig}\rangle = -\frac{\langle\alpha_g\rangle\langle\alpha_g\rangle^3\Delta\rho g}{\langle\langle v_{gj}\rangle\rangle^2}|\langle v_r\rangle|\langle v_r\rangle \tag{17}$$

where $\Delta\rho$ and v_{gj} are the density difference between two phases and drift velocity, respectively. The area-averaged relative velocity is calculated by Ref. [17]:

$$\langle v_r\rangle = C'_\alpha\left(\frac{1 - C_0\langle\alpha_g\rangle}{1 - \langle\alpha_g\rangle}\langle\langle v_g\rangle\rangle - C_0\langle\langle v_f\rangle\rangle\right) \tag{18}$$

In Eq. (18), the relative velocity covariance, C'_α, is defined by:

$$C'_\alpha \equiv \frac{1 - \langle\alpha_g\rangle}{1 - C_\alpha\langle\alpha_g\rangle} \tag{19}$$

where the void fraction covariance, C_α, is defined by:

$$C_\alpha \equiv \frac{\langle\alpha_g^2\rangle}{\langle\alpha_g\rangle\langle\alpha_g\rangle} \tag{20}$$

The distribution parameter, C_0, is defined by:

$$C_0 \equiv \frac{\langle\alpha_g j\rangle}{\langle\alpha_g\rangle\langle j\rangle} \tag{21}$$

where j is the mixture volumetric flux.

An approximate form with $C'_\alpha \simeq 1$ is currently used in computational codes [6–9] as:

$$\langle v_r\rangle \simeq \left(\frac{1 - C_0\langle\alpha_g\rangle}{1 - \langle\alpha_g\rangle}\langle\langle v_g\rangle\rangle - C_0\langle\langle v_f\rangle\rangle\right) \tag{22}$$

which is reasonable when the void fraction is low.

The drag coefficient approach is given as [2]:

$$\langle M_{ig}\rangle = -\frac{1}{8}\langle a_i\rangle C_D\rho_f|\langle v_r\rangle|\langle v_r\rangle \tag{23}$$

where a_i and C_D are the interfacial area concentration and drag coefficient, respectively.

In the drift velocity approach, the interfacial drag force is formulated by balancing the buoyancy force with the drag forces. The drift velocity approach couples the gas phase with the liquid phase and can provide a stable computation. In a strict sense, the drift velocity approach is valid under a steady-state condition. It should be noted here that the drift velocity approach does not apply to a horizontal flow. Although the drag coefficient approach is a mechanistic formulation, the drag coefficient approach requires accurate interfacial area concentration prediction, which is currently one of the weakest links in the code calculation [18,19]. The interfacial drag models in some system codes can be summarized as follows.

- RELAP5/MOD3 [6]: The drift velocity approach is used in bubbly and slug flow regimes for vertical two-phase flows. The drag coefficient approach is used in all flow regimes except for bubbly and slug flow regimes for vertical two-phase flows.
- TRACE V5 [8]: The drift velocity approach is used for vertical two-phase flows, and the TRACE does not explicitly consider the modeling of dispersed bubbly flow in a horizontal channel. In other words, the interfacial drag force model for vertical bubbly flows is also used for computing the interfacial drag force for horizontal bubbly flows.

- SPACE [12]: The drift velocity approach is used for bubbly, cap-bubbly, and slug flow regimes in vertical channels, including rod bundle and pipe. For other flow regimes, the drag coefficient approach is used.

3. Comparison of code calculations with horizontal flow data

3.1. Horizontal flow data

The measurement data for the discussion on comparing code calculations with horizontal flow data were collected by Talley et al. [20]. Talley et al. conducted an air-water bubbly flow experiment in a horizontal round channel under atmospheric pressure conditions. The inner diameter of the round channel, D, was 38.1 mm, and the channel length, L, was 248 times the channel diameter. Local void fraction, interfacial area concentration, and gas velocity were measured by a four-sensor conductivity probe. The axial locations for the measurements were $z/D = 44$, 116, and 244, where z is the axial distance from the test section inlet. The locally measured data were integrated over the flow channel to obtain the area-averaged values. The area-averaged superficial gas velocities obtained by the four-sensor probe agreed with those measured by a rotameter within ±10%.

Table 1 summarizes the test conditions. Talley et al. [20] presented the data of pressure, p, void fraction-weighted mean gas velocity, $\langle\langle v_g\rangle\rangle$, area-averaged void fraction, $\langle\alpha_g\rangle$, and area-averaged interfacial area concentration, $\langle a_i\rangle$, in figures. Those data were collected from the figures, and the area-averaged superficial gas velocity, $\langle j_g\rangle$, was calculated from $\langle\alpha_g\rangle\langle\langle v_g\rangle\rangle$. Table 1 summarizes the data measured at each z/D, including superficial liquid and gas velocities, pressure, void fraction, and interfacial area concentration. A total of 27 area-averaged data is collected. The test conditions in the experiment covered the superficial liquid velocity from 4.00 to 6.00 m/s, superficial gas velocity from 0.0745 to 0.561 m/s, void fraction from 0.0139 to 0.102, and interfacial area concentration from 62.5 to 419 m^{-1}. The slip ratio, S, can be determined from the collected data as:

Table 1
Test conditions in the horizontal bubbly flow experiment performed by Talley et al. [20].

Run #	z/D [−]	$\langle j_f\rangle$ [m/s]	$\langle j_g\rangle$ [m/s]	p [Pa]	$\langle\alpha_g\rangle$ [−]	$\langle a_i\rangle$ [m^{-1}]
1	44	4.00	0.104	165	0.0318	93.9
1	116	4.00	0.105	155	0.0341	106
1	244	4.00	0.113	138	0.0372	111
2	44	4.00	0.143	165	0.0466	131
2	116	4.00	0.158	155	0.0581	183
2	244	4.00	0.190	138	0.0652	183
3	44	5.00	0.0847	189	0.0204	77.6
3	116	5.00	0.0852	175	0.0205	82.6
3	244	5.00	0.114	150	0.0264	99.2
4	44	5.00	0.132	190	0.0323	120
4	116	5.00	0.135	176	0.0325	128
4	244	5.00	0.181	151	0.0422	156
5	44	5.00	0.251	194	0.0602	201
5	116	5.00	0.251	180	0.0603	225
5	244	5.00	0.348	154	0.0779	267
6	44	6.00	0.0745	220	0.0139	62.5
6	116	6.00	0.0755	200	0.0143	62.5
6	244	6.00	0.0864	166	0.0166	76.1
7	44	6.00	0.126	221	0.0245	96.9
7	116	6.00	0.127	201	0.0239	102
7	244	6.00	0.136	166	0.0262	116
8	44	6.00	0.237	226	0.0456	186
8	116	6.00	0.250	205	0.0464	191
8	244	6.00	0.286	170	0.0537	230
9	44	6.00	0.450	235	0.0843	314
9	116	6.00	0.479	214	0.0862	340
9	244	6.00	0.561	176	0.102	419

$$S = \frac{\langle\langle v_g\rangle\rangle}{\langle\langle v_f\rangle\rangle} = \frac{1-\langle\alpha_g\rangle}{\langle\alpha_g\rangle}\frac{\langle j_g\rangle}{\langle j_f\rangle} \tag{24}$$

3.2. Comparison of code calculations with data

The code calculations for the horizontal bubbly flow data collected in section 3.1 were conducted by Lee et al. [13]. Lee et al. performed the calculations using RELAP5/MOD3, TRACE V5, and SPACE codes. The calculated flow parameters were the pressure drop between $z/D = 116$ and 244, slip ratio at $z/D = 116$ and 244, and void fraction at $z/D = 116$ and 244.

3.2.1. Pressure drop

Fig. 2 shows the comparison of measured pressure drops between $z/D = 116$ and 244 and code calculations. Open black circles, red triangles, and green squares indicate the data collected at $\langle j_f\rangle = 4.0$, 5.0, and 6.0 m/s, respectively. Solid black, broken red, and dotted green lines are calculated by RELAP5, SPACE, and TRACE codes, respectively. Here, two statistical parameters, such as mean relative deviation, m_{rel}, and mean absolute relative deviation, $m_{rel,ab}$, are defined as Eqs. (25) and (26), respectively.

$$m_{rel} = \frac{\sum_{j=1}^{N}\left(\alpha_{g,cal,j} - \alpha_{g,exp,j}\right)}{\alpha_{g,exp,j}} \times 100 \tag{25}$$

$$m_{rel,ab} = \frac{\sum_{j=1}^{N}\left|\alpha_{g,cal,j} - \alpha_{g,exp,j}\right|}{\alpha_{g,exp,j}} \times 100 \tag{26}$$

where the subscripts of *cal.* and exp. indicate the calculated and experimental values, respectively. The mean relative deviation and mean absolute relative deviation reflect a bias and a random

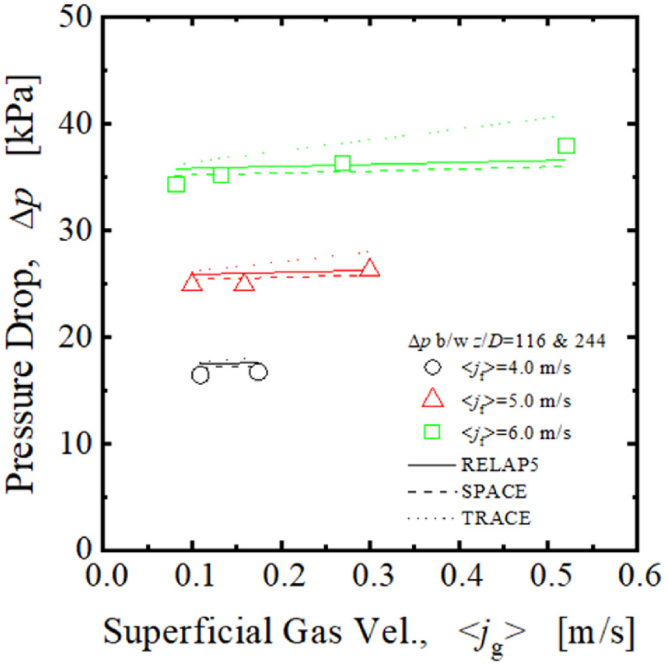

Fig. 2. Comparison of pressure drop data with code calculations.

uncertainty of a code calculation, respectively. A positive or negative value of the mean relative deviation indicates the overestimation or underestimation by the code, respectively. A large value of the mean absolute relative deviation indicates more scatter of the calculated value.

The mean relative deviations (bias) are 2.43, 0.605, and 6.35% for RELAP5, SPACE, and TRACE codes, respectively. The mean absolute relative deviations (random uncertainty) are 3.38, 2.69, and 6.35% for RELAP5, SPACE, and TRACE codes, respectively. All codes tend to overestimate the pressure drop, and the SPACE code provides the best predictive capability.

3.2.2. Slip ratio

Fig. 3 shows the comparison of experimental slip ratios and code calculations. Open black circles, red triangles, and green squares indicate the data collected at $\langle j_f \rangle = 4.0$, 5.0, and 6.0 m/s, respectively. Solid black, broken red, and dotted green lines are calculated by RELAP5, SPACE, and TRACE codes, respectively. The mean relative deviations (bias) are 29.5, 25.4, and 42.2% for RELAP5, SPACE, and TRACE codes, respectively. The mean absolute relative deviations (random uncertainty) are 29.5, 25.4, and 42.2% for RELAP5, SPACE, and TRACE codes, respectively. The slip ratios obtained in the experiment are lower than unity, and all codes tend to overestimate the slip ratio significantly. In what follows, the cause of the slip ratio lower than unity is discussed.

The void fraction is expressed by the slip ratio as:

$$\langle \alpha_g \rangle = \frac{1}{1 + \frac{1-\langle x \rangle}{\langle x \rangle} \frac{\rho_g}{\rho_f} S} \tag{27}$$

where $\langle x \rangle$ is the quality.

The one-dimensional drift-flux model is expressed as:

$$\langle\langle v_g \rangle\rangle = C_0 \langle j \rangle + \langle\langle v_{gj} \rangle\rangle \tag{28}$$

The void fraction is also expressed in a drift-flux model form as:

$$\langle \alpha_g \rangle = \frac{1}{C_0 \left(1 + \frac{1-\langle x \rangle}{\langle x \rangle} \frac{\rho_g}{\rho_f} \right) + \frac{\langle\langle v_{gj} \rangle\rangle \rho_g}{G \langle x \rangle}} \tag{29}$$

where G is the mass flux.

Equating Eqs. (27) and (29) yields:

$$S = C_0 + (C_0 - 1) \frac{\langle j_g \rangle}{\langle j_f \rangle} + \frac{\langle\langle v_{gj} \rangle\rangle}{\langle j_f \rangle} \tag{30}$$

For horizontal bubbly flows, local velocity slip may be approximated to be zero, resulting in $\langle\langle v_{gj} \rangle\rangle \simeq 0$. Therefore, Eq. (30) is simplified for horizontal bubbly flows as:

$$S \simeq 1 - \frac{1 - C_0}{1 - C_0 \langle \alpha \rangle} \tag{31}$$

Fig. 4 shows the dependence of the slip ratio for horizontal bubbly flows on the void fraction for a fixed distribution parameter, which is calculated by Eq. (31). Solid black, broken red, and dotted green lines are the slip ratios calculated by Eq. (31) with $C_0 = 1.2$, 1.0, 0.8, respectively. The figure indicates that the slip ratio is lower than unity when the distribution parameter is lower than unity. By assuming no local velocity slip, the distribution parameter can be calculated from the drift-flux model as:

$$C_0 = \frac{\langle\langle v_g \rangle\rangle}{\langle j \rangle} \tag{32}$$

Fig. 5 shows the dependence of the distribution parameter for horizontal bubbly flows on the void fraction. Open black circles, red triangles, and green squares indicate the distribution parameters calculated by Eq. (32) at $\langle j_f \rangle = 4.0$, 5.0, and 6.0 m/s, respectively. The figure indicates that the distribution parameters in the experiment are lower than unity. Talley et al. [20] measured the void fraction distribution in the circular channel and demonstrated that the gas phase was localized near the top of the test section due to the buoyancy force acting on the gas phase. The localized gas phase near the top of the test section decreases the distribution parameter (see Appendix A). Since the code calculations of the pressure drop agree with the data within 10%, the significant discrepancy in the slip ratio between the code calculations and data may be attributed to inaccurate modeling of the interfacial drag force.

3.2.3. Void fraction

Fig. 6 shows the comparison of measured area-averaged void fraction and code calculations. Open black circles, red triangles, and green squares indicate the data collected at $\langle j_f \rangle = 4.0$, 5.0, and 6.0 m/s, respectively. Solid black, broken red, and dotted green lines are calculated by RELAP5, SPACE, and TRACE codes, respectively. The mean relative deviations (bias) are −20.2, −18.4, and −29.2% for RELAP5, SPACE, and TRACE codes, respectively. The mean

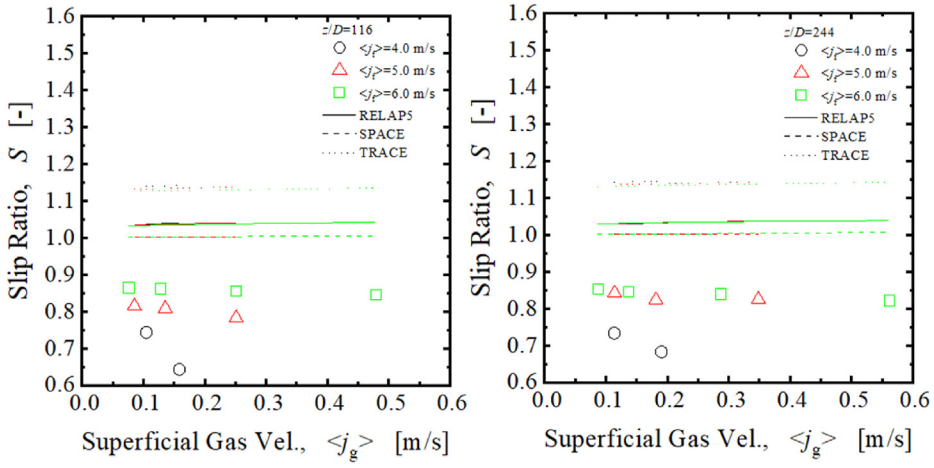

Fig. 3. Comparison of slip ratio data with code calculations.

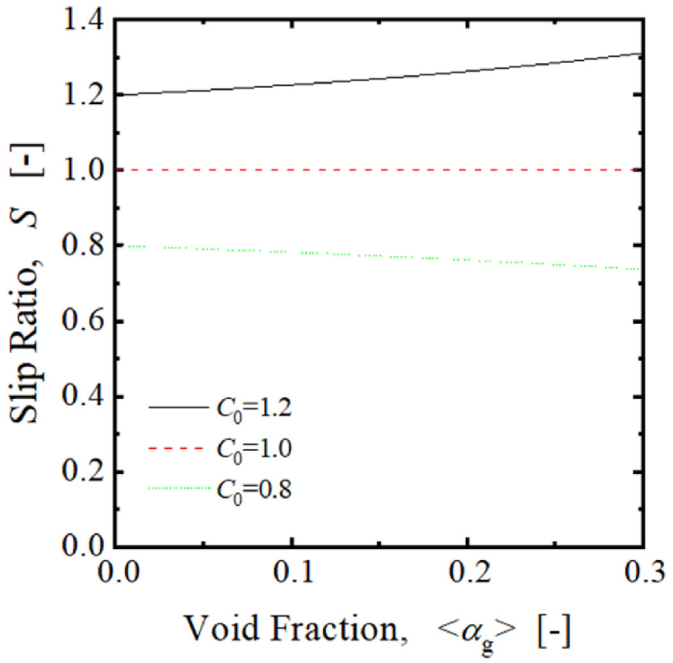

Fig. 4. Dependence of slip ratio for horizontal bubbly flows on void fraction for fixed distribution parameter.

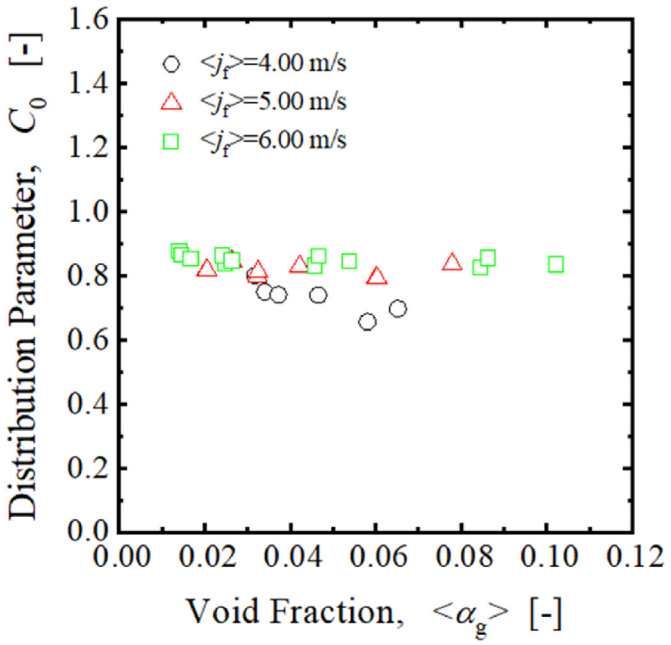

Fig. 5. Dependence of distribution parameter for horizontal bubbly flows on void fraction.

absolute relative deviations (random uncertainty) are 20.2, 18.4, and 29.2% for RELAP5, SPACE, and TRACE codes, respectively. Thus, all codes tend to underestimate the void fraction significantly. As shown in Eq. (27), the underestimation of the void fraction is consistent with the overestimation of the slip ratio.

4. Formulation of partition method of wall friction in a one-dimensional two-fluid model

4.1. Momentum equation in two-fluid model

The momentum equation of k-phase in the two-fluid model is expressed by Ref. [2]:

$$\frac{\partial \alpha_k \rho_k \mathbf{v}_k}{\partial t} + \nabla\cdot(\alpha_k \rho_k \mathbf{v}_k \mathbf{v}_k) = -\alpha_k \nabla p_k + \nabla\cdot\left\{\alpha_k\left(\mathrm{T}_k + \mathrm{T}_k^T\right)\right\} + \alpha_k \rho_k \mathbf{g}_k + \mathbf{v}_{ki}\Gamma_k + \mathbf{M}_{ik} - \nabla\alpha_k\cdot\mathrm{T}_{ki} + (p_{ki} - p_k)\nabla\alpha_k \tag{33}$$

where T_k, T_k^T and Γ_k are the viscous stress, turbulent stress, and mass generation rate per unit volume of k-phase, respectively. The subscript, i, means the quantity at the interface. The one-dimensional momentum equation can be obtained by integrating Eq. (33) over a flow channel area as [22]:

$$\frac{\partial\langle\alpha_k\rangle\rho_k\langle\langle v_k\rangle\rangle}{\partial t} + \frac{\partial}{\partial z}C_{vk}\langle\alpha_k\rangle\rho_k\langle\langle v_k\rangle\rangle^2 = -\langle\alpha_k\rangle\frac{\partial p_k}{\partial z} + \frac{\partial}{\partial z}\langle\alpha_k\rangle\langle\langle\tau_{kzz} + \tau_{kzz}^T\rangle\rangle - \frac{4}{D_H}\alpha_{kw}\tau_{kw} - \langle\alpha_k\rangle\rho_k g_z + \langle\langle v_{ki}\rangle\rangle\langle\Gamma_k\rangle + \langle\mathbf{M}_{ik}\rangle_z - \langle\nabla\alpha_k\cdot\mathrm{T}_{ki}\rangle_z + \langle(p_{ki} - p_k)\frac{\partial\alpha_k}{\partial z}\rangle. \tag{34}$$

The magnitude of the covariance, C_{vk}, can be estimated as follows [22]. For bubbly, slug and churn-turbulent flows,

$$C_{vk} \simeq \begin{cases} 1 + 0.5(C_0 - 1) \text{ for gas phase} \\ 1 + 1.5(C_0 - 1) \text{ for liquid phase} \end{cases} \tag{35}$$

For annular flow,

$$C_{vk} \simeq \begin{cases} 1.02 \text{ for turbulent flow} \\ 1.33 \text{ for laminar flow} \end{cases} \tag{36}$$

Equations (35) and (36) suggest that the magnitude of the covariance term is close to unity.

The sixth and seventh terms on the right-hand side of Eq. (34) are grouped as the total interfacial drag force per unit volume, $\langle\mathbf{M}_k^d\rangle_z$.

$$\langle\mathbf{M}_k^d\rangle_z \equiv \langle\mathbf{M}_{ik}\rangle_z - \langle\nabla\alpha_k\cdot\mathrm{T}_{ki}\rangle_z \tag{37}$$

The first term on the right-hand side of Eq. (37) expresses the generalized particle drag. The second term considers the effects of void fraction gradient and interfacial shear on the total interfacial drag force per unit volume. The first and second terms are essential for a dispersed and separated flow, respectively.

Equation (34) can be simplified as Eq. (38) under the assumptions of an adiabatic condition and $p_{ki} \simeq p_k$.

$$\frac{\partial\langle\alpha_k\rangle\rho_k\langle\langle v_k\rangle\rangle}{\partial t}+\frac{\partial}{\partial z}C_{vk}\langle\alpha_k\rangle\rho_k\langle\langle v_k\rangle\rangle^2=-\langle\alpha_k\rangle\frac{\partial p_k}{\partial z}-\langle\mathbf{M}_{\tau k}\rangle_z-\frac{4}{D_H}\alpha_{kw}\tau_{kw}-\langle\alpha_k\rangle\rho_k g_z+\langle\mathbf{M}_{ik}\rangle_z-\langle\nabla\alpha_k\cdot\mathrm{T}_{ki}\rangle_z \tag{38}$$

where τ_w and D_H are the wall shear force and hydraulic equivalent diameter, respectively, and

$$\langle\mathbf{M}_{\tau k}\rangle_z\equiv-\frac{\partial}{\partial z}\left(\langle\alpha_k\rangle\langle\langle\tau_{kzz}+\tau^T_{kzz}\rangle\rangle\right) \tag{39}$$

Since the dominant viscous force and turbulent shear force should be z-component acting on the r-surface, τ_{kzz} and τ^T_{kzz} should be negligibly small. Thus, $\langle\mathbf{M}_{\tau k}\rangle_z$ should be negligibly small (see Appendix B). The void fraction at the wall is assumed to be zero.

4.2. One-dimensional momentum equation for bubbly, slug and churn-turbulent flow regimes

For the bubbly, slug and churn-turbulent flows, the last term on the right-hand side of Eq. (38) is modeled as [22]:

$$-\langle\nabla\alpha_g\cdot\mathrm{T}_i\rangle_z=-\frac{4\tau_w}{D_H}\langle\alpha_g\rangle C_\tau \tag{40}$$

where C_τ is expected to be very close to one and set at 1 here. The derivation of Eq. (40) is given in Appendix C.

Substituting Eq. (40) into Eq. (38) yields:

$$\frac{\partial\langle\alpha_g\rangle\rho_g\langle\langle v_g\rangle\rangle}{\partial t}+\frac{\partial}{\partial z}\langle\alpha_g\rangle\rho_g\langle\langle v_g\rangle\rangle^2=-\langle\alpha_g\rangle\frac{\partial p_g}{\partial z}-\langle\alpha_g\rangle\rho_g g_z+\langle\mathbf{M}_{ig}\rangle_z-\langle\alpha_g\rangle F_w \tag{41}$$

where $F_w=4\tau_w/D_H$.

$$\begin{aligned}\frac{\partial\langle\alpha_f\rangle\rho_f\langle\langle v_f\rangle\rangle}{\partial t}+\frac{\partial}{\partial z}\langle\alpha_f\rangle\rho_f\langle\langle v_f\rangle\rangle^2&=-\langle\alpha_f\rangle\frac{\partial p_f}{\partial z}-\frac{4}{D_H}\tau_{fw}-\langle\alpha_f\rangle\rho_f g_z+\langle\mathbf{M}_{if}\rangle_z+\frac{4\tau_w}{D_H}\langle\alpha_g\rangle\\&=-\langle\alpha_f\rangle\frac{\partial p_f}{\partial z}-\frac{4}{D_H}\tau_{fw}(1-\langle\alpha_g\rangle)-\langle\alpha_f\rangle\rho_f g_z+\langle\mathbf{M}_{if}\rangle_z\\&=-\langle\alpha_f\rangle\frac{\partial p_f}{\partial z}-\langle\alpha_f\rangle\rho_f g_z+\langle\mathbf{M}_{if}\rangle_z-\langle\alpha_f\rangle F_w\end{aligned} \tag{42}$$

Equations (41) and (42) are consistent with the partition method of the wall friction adopted in the SPACE code [14]. It should be noted here that, in the TRACE code, the wall friction in bubbly, slug, and churn-turbulent flow regimes is totally imposed to the liquid phase. This induced more significant deviations of the TRACE calculations from the measured pressure drops in Section 3.

4.3. One-dimensional momentum equation for annular flow regime

For the annular flows, the last term on the right-hand side of Eq. (38) is modeled as [22]:

$$-\langle\nabla\alpha_k\cdot\mathrm{T}_i\rangle_z=-\frac{\xi_i}{A}\tau_{gi} \tag{43}$$

where ξ_i is the wetted perimeter of the gas core. The derivation of Eq. (43) is given in Appendix D. The constitutive equation for τ_{gi} is given by:

$$\tau_{gi}=\frac{f_i}{2}\rho_g\overline{v_r}|\overline{v_r}| \tag{44}$$

where

$$\overline{v_r}=\langle\langle v_g\rangle\rangle-\langle\langle v_f\rangle\rangle \tag{45}$$

The friction factor, f_i, can be given by:

$$f_i=0.005\{1+75(1-\langle\alpha_g\rangle)\} \tag{46}$$

Substituting Eq. (43) into Eq. (38) yields:

$$\frac{\partial\langle\alpha_g\rangle\rho_g\langle\langle v_g\rangle\rangle}{\partial t}+\frac{\partial}{\partial z}\langle\alpha_g\rangle\rho_g\langle\langle v_g\rangle\rangle^2=-\langle\alpha_g\rangle\frac{\partial p_g}{\partial z}-\langle\alpha_g\rangle\rho_g g_z+\langle\mathbf{M}_{ig}\rangle_z-\frac{\xi_i}{A}\tau_{gi} \tag{47}$$

$$\frac{\partial\langle\alpha_f\rangle\rho_f\langle\langle v_f\rangle\rangle}{\partial t}+\frac{\partial}{\partial z}\langle\alpha_f\rangle\rho_f\langle\langle v_f\rangle\rangle^2=-\langle\alpha_f\rangle\frac{\partial p_f}{\partial z}-\frac{4}{D}\tau_{fw}-\langle\alpha_f\rangle\rho_f g_z+\langle\mathbf{M}_{if}\rangle_z+\frac{\xi_i}{A}\tau_{gi} \tag{48}$$

In pure annular flow, $\langle\mathbf{M}_{ik}\rangle_z=0$.

4.4. One-dimensional momentum equation for mist flow regime

In the bubbly, slug, and churn-turbulent flow formulation, Eqs. (41) and (42) are the momentum equations for the dispersed gas and continuous liquid phases, respectively. Equations (41) and (42) apply to the mist flow. In the mist flow formulation, Eqs. (41) and (42) are the momentum equations for the continuous gas and dispersed liquid phases, respectively. The detailed derivation is given in Appendix E.

5. Constitutive equations necessary for formulating interfacial drag force

As indicated by Eqs. (18) and (23), several constitutive equations are necessary for calculating the interfacial drag force. They are the equations for the distribution parameter, interfacial area concentration, relative velocity covariance, and drag coefficient. Since the drag coefficient model [23] is well-established, state-of-the-art correlations for the distribution parameter, interfacial area concentration, and relative velocity covariance are discussed below.

5.1. Drift-flux correlation and its validity

Rassame and Hibiki [15] developed the one-dimensional drift-flux correlation for two-phase flows in horizontal pipes given by:

$$\langle\langle v_g\rangle\rangle=C_0\langle j\rangle \tag{49}$$

where

$$C_0 = 0.800 \exp\left\{0.815\left\{\frac{\langle j_g^+\rangle / \langle j^+\rangle}{0.900}\right\}^{1.50}\right\}$$

$$-\left[0.800 \exp\left\{0.815\left\{\frac{\langle j_g^+\rangle / \langle j^+\rangle}{0.900}\right\}^{1.50}\right\} - 1\right]\sqrt{\frac{\rho_g}{\rho_f}} \text{ for } 0 \le \langle j_g^+\rangle / \langle j^+\rangle < 0.9 \quad (50)$$

$$C_0 = \left(-8.08\langle j_g^+\rangle / \langle j^+\rangle + 9.08\right)$$

$$-8.08\left(\langle j_g^+\rangle / \langle j^+\rangle + 1\right)\sqrt{\frac{\rho_g}{\rho_f}} \text{ for } 0.9 \le \langle j_g^+\rangle / \langle j^+\rangle \le 1$$

The non-dimensional superficial gas velocity and mixture volumetric flux are defined as:

$$\langle j_g^+\rangle \equiv \frac{\langle j_g\rangle}{\left(\frac{\Delta\rho g\sigma}{\rho_f^2}\right)^{1/4}} \text{ and } \langle j^+\rangle \equiv \frac{\langle j\rangle}{\left(\frac{\Delta\rho g\sigma}{\rho_f^2}\right)^{1/4}} \quad (51)$$

where σ is the surface tension. The Rassame-Hibiki correlation was validated by 566 data points collected in a wide range of test conditions such as superficial gas velocity ranging from 0.0253 to 47.5 m/s, superficial liquid velocity ranging from 0.000057 to 5.97 m/s, inner pipe diameter ranging from 0.019 to 0.0779 m, and void fraction ranging from ~0 to ~1.

Fig. 7 compares void fraction data for horizontal bubbly flows [20] with the Rassame-Hibiki correlation. Open black circles, red triangles, and green squares indicate the data collected at $\langle j_f\rangle = 4.0$, 5.0, and 6.0 m/s, respectively. The Rassame-Hibiki correlation agrees with the data well. The mean relative deviation (bias) and mean absolute relative deviations (random uncertainty) of the Rassame-Hibiki correlation for the horizontal bubbly flow data [20] are 0.918% and 5.32%, respectively.

The Chexal-Lellouche correlation [21] is also applicable to predicting void fraction in horizontal two-phase flows. Rassame and Hibiki [15] evaluated the prediction accuracy of the Chexal-Lellouche correlation for the dispersed bubbly flow regime in horizontal channels. The mean relative deviation (bias) and mean absolute relative deviations (random uncertainty) of the Chexal-Lellouche correlation for the horizontal dispersed bubbly flow data are 10.1% and 10.1%, respectively. The Chexal-Lellouche correlation tends to overestimate the void fraction in the dispersed bubbly flow regime. These two evaluation results indicate that the Rassame-Hibiki correlation gives void fraction prediction better than the Chexal-Lellouche correlation.

5.2. Interfacial area concentration correlation and its validity

The correlation of one-dimensional interfacial area concentration for the bubbly flows is given by Ref. [25]:

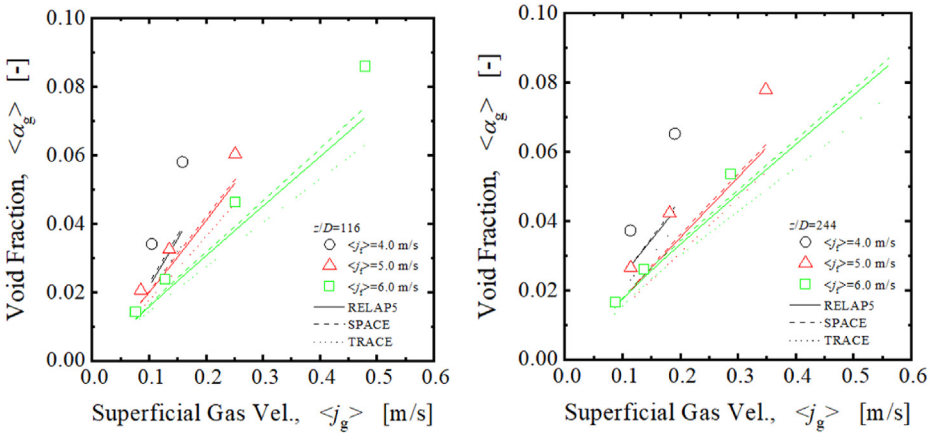

Fig. 6. Comparison of void fraction data with code calculations.

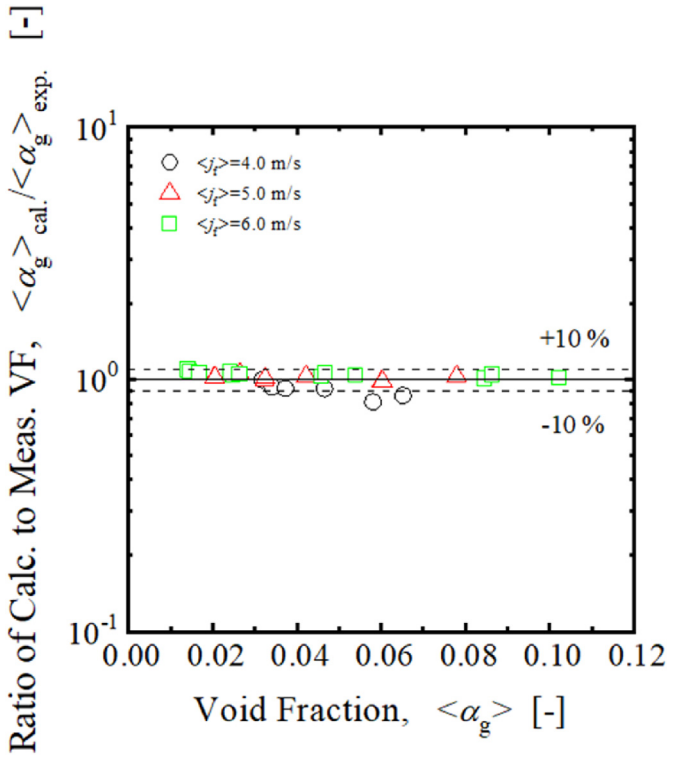

Fig. 7. Comparison of void fraction data with Rassame-Hibiki correlation.

$$\langle a_i \rangle = \frac{3.02 g^{0.174}}{D_H^{0.335} \nu_f^{0.239}} \left(\frac{\sigma}{\Delta \rho} \right)^{-0.174} \langle \alpha_g \rangle \langle \varepsilon \rangle^{0.0796} \tag{52}$$

where ν_f and ε are the kinematic viscosity and energy dissipation rate per unit mass, respectively. The Hibiki and Ishii correlation was validated by 459 data collected in bubble columns and forced bubbly convective flows under various conditions. The database covered the conditions such as channel geometry (circular and rectangular channels), channel hydraulic equivalent diameter (9.0–5500 mm), flow direction (vertical and horizontal flows), superficial gas velocity (0.000788–4.87 m/s), and superficial liquid velocity (0.00–6.55 m/s). The mean absolute relative deviations (random uncertainty) of the Hibiki-Ishii correlation was reported to be 22.0%. When the Hibiki-Ishii correlation is applied to horizontal bubbly flows, the gravitational acceleration should be set at the nominal value (=9.8 m/s^2).

Fig. 8 compares the interfacial area concentration data for horizontal bubbly flows [20] with the Hibiki-Ishii correlation. Open black circles, red triangles, and green squares indicate the data collected at $\langle j_f \rangle$ = 4.0, 5.0, and 6.0 m/s, respectively. The Hibiki-Ishii correlation tends to underestimate the interfacial area concentration data slightly. The mean relative deviation (bias) and mean absolute relative deviations (random uncertainty) of the Hibiki-Ishii correlation for the horizontal bubbly flow data [20] are −32.1 and 32.1%, respectively. The prediction accuracy (=32.1%) for the data collected by Talley et al. is similar to the one (=22.0%) reported by Hibiki and Ishii [22]. If a 30% error is accepted, the Hibiki-Ishii correlation is still applicable to horizontal bubbly flows. The 30% error may be acceptable because of the difficulty in predicting the interfacial area concentration.

Fig. 8 also includes the comparison between RELAP5 interfacial area concentration correlation, Eq. (53), and the data collected by Talley et al. The RELAP5 interfacial area concentration correlation is given by:

$$\langle a_i \rangle = \frac{3.6 \langle \alpha_g \rangle}{D_0} = \frac{7.2 \langle \alpha_g \rangle}{D_{\max}} \tag{53}$$

where

$$N_{We} = \frac{D_{\max} \rho_f \left(\langle \langle v_g \rangle \rangle - \langle \langle v_f \rangle \rangle \right)^2}{\sigma} \tag{54}$$

The Weber number for the bubbly flow regime is set at 10.0.

Solid black circles, red triangles, and green squares indicate the data collected at $\langle j_f \rangle$ = 4.0, 5.0, and 6.0 m/s, respectively. The RELAP5 interfacial area concentration correlation significantly overestimates the data. The mean relative deviation (bias) and mean absolute relative deviations (random uncertainty) of the RELAP5 correlation for the horizontal bubbly flow data [20] are 196 and 196%, respectively.

The correlation of the interfacial area concentration, Eq. (53), in the RELAP5 code fails to predict the interfacial area concentration data for horizontal bubbly flows. The SPACE code implemented the correlation of Hibiki et al. [23] to predict the interfacial area concentration in the bubbly flow regime. The correlation of Hibiki et al. (2006) is the advanced version of the Hibiki-Ishii correlation, which applies to predicting the interfacial area concentration of boiling bubbly flows under real nuclear reactor conditions. The correlation of Hibiki et al. is reduced to the Hibiki-Ishii correlation under adiabatic flow conditions. The Hibiki-Ishii correlation implemented in the SPACE code reasonably predicts the interfacial area concentration for horizontal bubbly flows. Since the TRACE code adopts the drift velocity approach in calculating the interfacial drag force, it does not use the correlation of the interfacial area concentration in calculating the interfacial drag force.

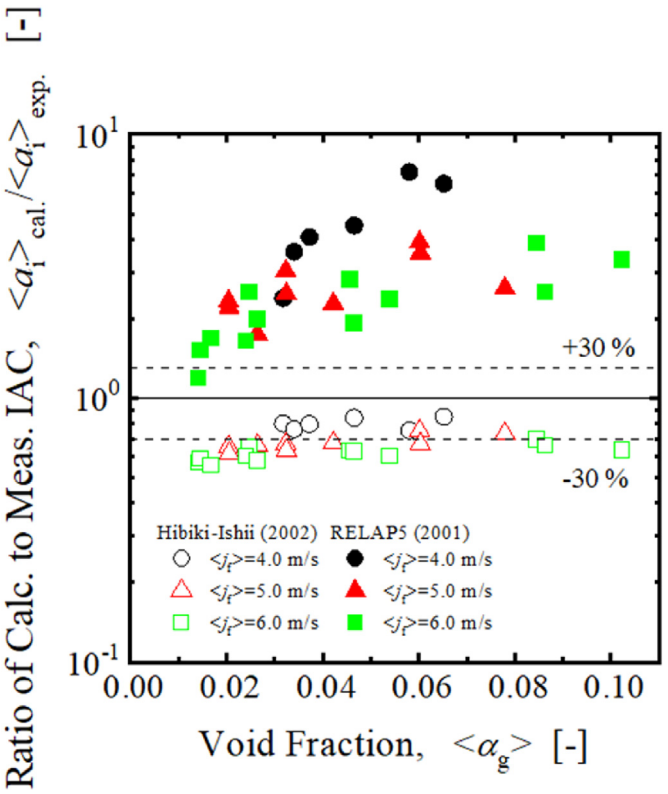

Fig. 8. Comparison of interfacial area concentration data with Hibiki-Ishii correlation and RELAP5 correlation.

5.3. Relative velocity covariance correlation and its validity

Rassame and Hibiki [27] have modeled the relative velocity covariance model for horizontal flows as:

$$C'_{\alpha} \equiv \frac{1-\langle \alpha_g \rangle}{1-\left(2.38-1.38\sqrt{\frac{\rho_g}{\rho_f}}\right)\langle \alpha_g \rangle} \tag{55}$$

For low void fraction cases, the relative velocity covariance may be approximated to be unity. The drag coefficient is given by Ishii and Zuber [23]. The sensitivity analysis on the wall frictional force modeling should be performed with the accurate formulation of the interfacial drag force.

6. Conclusions

This paper discussed the fundamental issues in void fraction prediction using a one-dimensional nuclear thermal-hydraulic system analysis code based on the two-fluid model. The key constitutive equations predicting the void fraction were the interfacial drag force model and partitioning of wall friction to each phase. The discussions, findings, and recommendations obtained in this study are summarized as follows.

- Partition methods of wall friction adopted in safety analysis codes were briefly reviewed. The TRACE code imposed total wall friction to the liquid phase for bubbly, slug, and annular/mist flows. The SPACE code apportioned total wall friction to gas and liquid phases based on phasic volume fraction, such as void fraction and liquid fraction. The RELAP5 code partitioned total wall friction based on a technique derived by Chisholm [24] from the Lockhart-Martinelli model [25]. A sample calculation performed for a horizontal two-phase flow under the condition of the superficial liquid velocity of 2 m/s and pressure of 7.0 MPa demonstrated that the RELAP5 code treatment was in-between the TRACE and SPACE code treatments.
- The area-averaged relative velocity of a horizontal bubbly flow might be positive for the TRACE and RELAP5 code treatments. The relative velocity might be zero for the SPACE code treatment.
- Two approaches, such as the drift velocity approach and drag coefficient approach, were reviewed to formulate the interfacial drag force. It was pointed out that the drift velocity approach currently used in the TRACE code did not apply to a horizontal two-phase flow.
- Code calculations performed by Lee et al. [13] were compared with horizontal bubbly flow data collected in a horizontal channel with an inner diameter of 38.1 mm [20]. Experimentally observed slip ratios and distribution parameters were significantly lower than unity due to the localized gas phase around the top of the horizontal test section induced by the buoyancy force. All codes tended to overestimate the slip ratio and underestimate the void fraction.
- The one-dimensional momentum equation in the two-fluid model was derived from the local momentum equation. The derived one-dimensional momentum equation demonstrated that the total wall friction should be apportioned to both gas and liquid phases based on the phasic volume fraction. The derived one-dimensional momentum equation was the same as that adopted in the SPACE code.
- The constitutive equations necessary for formulating the interfacial drag force were identified and were the equations for the distribution parameter, interfacial area concentration, drag coefficient, and relative velocity covariance. The Rassame-Hibiki correlation [15], Hibiki-Ishii correlation [22], Ishii-Zuber correlation [26], and Rassame-Hibiki correlation [27] were recommended for computing the distribution parameter, interfacial area concentration, drag coefficient, and relative velocity covariance of a horizontal bubbly flow, respectively.
- Sensitivity calculations are recommended for optimizing the interfacial drag force model in a future study.

Declaration of competing interest

The authors declare that they have no known competing financial interests or personal relationships that could have appeared to influence the work reported in this paper.

Acknowledgment

The work described in this paper was partially supported by a grant from City University of Hong Kong (Project No. 9380126) and Global STEM Professorship, Hong Kong. One of the authors (T. Hibiki) appreciates the support.

Nomenclature

a_i	interfacial area concentration
C_D	drag coefficient
C_i	overall drag coefficient
C_v	covariance in momentum convection term
C_α	void fraction covariance
C'_α	relative velocity covariance
C_τ	coefficient
C_0	distribution parameter
c	partition coefficient
$D_{\max}$	maximum bubble size
D_0	average bubble size
G	mass flux
F_w	wall friction force per unit volume
f_i	friction factor
g	gravitational acceleration
j	mixture volumetric flux
$\mathbf{M}^d$	total interfacial drag force
M_i	generalized interfacial drag force
M_w	wall friction
$M_{w2\phi}$	total two-phase wall friction
$\mathbf{M}_\tau$	Total of viscous and turbulent shear stresses
m	exponent
m_j	exponent
N_{We}	Weber number
n	exponent
p	pressure
R	channel radius
r	radial coordinate
S	slip ratio
s	scalar
t	time
v	velocity
v_f	liquid velocity
v_g	gas velocity
v_{gj}	drift velocity
v_r	relative velocity between two phases
$\overline{v_r}$	difference between void-fraction weighted mean gas and liquid velocities
x	quality
z	axial coordinate or distance from test section inlet

Greek symbol

α_g	void fraction
$\alpha_{g,b}$	void fraction in two-phase flow region
α_{fw}	void fraction at wall
α_{gw}	liquid fraction at wall
Γ_k	mass generation rate per unit volume
$\Delta\rho$	density difference between two phases
ε	energy dissipation rate per unit mass
θ	azimuthal coordinate
κ	Dilatational viscosity
λ	Darcy-Weisbach friction factor
μ	dynamic viscosity
ν_f	kinematic viscosity
ξ_i	wetted perimeter of gas core
ρ	density
σ	surface tension
T	tensor
T_k	viscous stress
T_k^T	turbulent stress
τ_i	interfacial shear stress
τ_w	wall shear stress

Subscripts

c	values at channel center
f	liquid phase
g	gas phase
i	quantity at interface
k	k-phase

Superscript

$+$	non-dimensional value

Appendix A

The purpose of Appendix A is to demonstrate that the localized gas phase near the top of the test section tends to decrease the distribution parameter. For this purpose, a simple two-dimensional horizontal channel with an infinite width is considered, as depicted in Fig. A1.

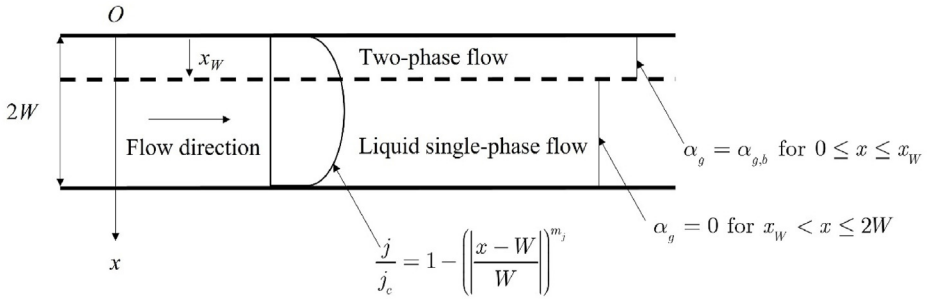

Fig. A1. Assumed distributions of void fraction and mixture volumetric flux.

The assumed distribution of the mixture volumetric flux is expressed by:

$$\frac{j}{j_c} = 1 - \left(\left|\frac{x-W}{W}\right|\right)^{m_j} \tag{A1}$$

where x, W, and m_j are the vertical distance measured from the top of the test section, half of the channel width, and exponent, respectively. The subscript, c, means the value at the channel center.

The assumed distribution of the void fraction is represented by:

$$\begin{cases} \alpha_g = \alpha_{g,b} \text{ for } 0 \le x \le x_W \\ \alpha_g = 0 \text{ for } x_W \le x \le 2W \end{cases} \tag{A2}$$

where $\alpha_{g,b}$ and x_W are the void fraction in the two-phase flow region and the vertical distance for the two-phase flow region measured from the top of the test section.

The area-averaged mixture volumetric flux is given by:

$$\langle j \rangle = \frac{m_j}{m_j+1} j_c \tag{A3}$$

The area-averaged void fraction is given by:

$$\langle \alpha_g \rangle = \frac{x_W}{2W} \alpha_{g,b} \tag{A4}$$

The area-averaged product of the void fraction and mixture volumetric flux is given by:

$$\langle \alpha_g j \rangle = \frac{j_c \alpha_{g,b}}{2} \left\{ \frac{m_j}{m_j+1} - \left(1 - \frac{2\langle \alpha_g \rangle}{\alpha_{g,b}}\right) + \frac{1}{m_j+1}\left(1 - \frac{2\langle \alpha_g \rangle}{\alpha_{g,b}}\right)\left(\left|1 - \frac{2\langle \alpha \rangle}{\alpha_{g,b}}\right|\right)^{m_j} \right\} \tag{A5}$$

Substituting Eq. (A3), (A4), and (A5) into Eq. (21) yields:

$$C_0 = \frac{\alpha_{g,b}}{2\langle \alpha_g \rangle} \left\{ 1 - \frac{m_j+1}{m_j}\left(1 - \frac{2\langle \alpha_g \rangle}{\alpha_{g,b}}\right) + \frac{1}{m_j}\left(1 - \frac{2\langle \alpha_g \rangle}{\alpha_{g,b}}\right)\left(\left|1 - \frac{2\langle \alpha_g \rangle}{\alpha_{g,b}}\right|\right)^{m_j} \right\} \tag{A6}$$

For stratified flows, $\alpha_{g,b} = 1$, resulting in:

$$C_0 = \frac{1}{2\langle \alpha_g \rangle} \left\{ 1 - \frac{m_j+1}{m_j}(1 - 2\langle \alpha_g \rangle) + \frac{1}{m_j}(1 - 2\langle \alpha_g \rangle)(|1 - 2\langle \alpha_g \rangle|)^{m_j} \right\} \tag{A7}$$

which is similar to the equation for the distribution parameter of oil-water stratified flow in horizontal channels developed by

Baotong et al. [27].

Figure A2 shows the distribution parameter calculated with assumed $\alpha_{g,b}$. Solid black, broken red, and dotted green lines are the values calculated with $\alpha_{g,b}$ = 0.1, 0.2, and 0.3, respectively. The figure demonstrates that the localized gas phase near the top of the test section decreases the distribution parameter.

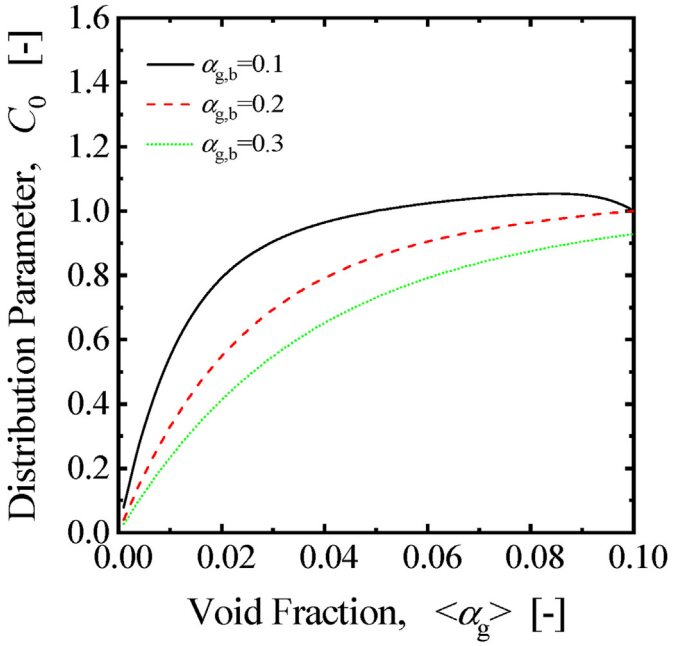

Fig. A2. Dependence of distribution parameter on void fraction.

Appendix B

The purpose of Appendix B is to demonstrate that $\langle \mathbf{M}_{\tau k} \rangle_z$ should be negligibly small. The z-component of the viscous stress is expressed by:

$$\tau_{zz} = -\mu\left(2\frac{\partial v_z}{\partial z}\right) + \left(\frac{2}{3}\mu - \kappa\right)(\nabla\cdot\mathbf{v}) \tag{B1}$$

where μ and κ are the dynamic viscosity and dilatational viscosity, respectively, and

$$\nabla\cdot\mathbf{v} = \frac{1}{r}\frac{\partial}{\partial r}(rv_r) + \frac{1}{r}\frac{\partial v_\theta}{\partial \theta} + \frac{\partial v_z}{\partial z} \simeq \frac{\partial v_z}{\partial z} \tag{B2}$$

where r and θ are the radial and azimuthal coordinates, respectively.

Substituting Eq. (B2) into Eq. (B1) yields:

$$\tau_{zz} = -\left(\frac{4}{3}\mu + \kappa\right)\frac{\partial v_z}{\partial z} \tag{B3}$$

The z-component of the viscous stress is a function of the velocity gradient of z-directional velocity along the z-direction. This term is generally small. Similarly, the z-component of the turbulent stress should be expressed as a function of the z-directional velocity along the z-direction. This term is also small in general. As can be seen in Eq. (39), $\langle \mathbf{M}_{\tau k} \rangle_z$ should be the function of the second-order of the z-directional velocity. Such a "diffusion" term should be negligibly small in general.

Appendix C

The purpose of Appendix C is to derive Eq. (40). Several vectors and tensor operations are required for the derivation.

$$\nabla\cdot(s\mathrm{T}) = \nabla s\cdot\mathrm{T} + s(\nabla\cdot\mathrm{T}) \tag{C1}$$

where s and T are a scalar and tensor, respectively.

The z-components of $\nabla\cdot(s\mathrm{T})$ and $\nabla\cdot\mathrm{T}$ are:

$$[\nabla\cdot(s\mathrm{T})]_z = \frac{1}{r}\frac{\partial}{\partial r}(rs\tau_{rz}) + \frac{1}{r}\frac{\partial}{\partial \theta}(s\tau_{\theta z}) + \frac{\partial}{\partial z}(s\tau_{zz}) \tag{C2}$$

$$[\nabla\cdot\mathrm{T}]_z = \frac{1}{r}\frac{\partial}{\partial r}(r\tau_{rz}) + \frac{1}{r}\frac{\partial}{\partial \theta}(\tau_{\theta z}) + \frac{\partial}{\partial z}(\tau_{zz}) \tag{C3}$$

Thus,

$$[\nabla s\cdot\mathrm{T}]_z = \tau_{rz}\frac{\partial s}{\partial r} + \frac{\tau_{r\theta}}{r}\frac{\partial s}{\partial \theta} + \tau_{zz}\frac{\partial s}{\partial z} \tag{C4}$$

By assuming $\alpha_g = \alpha_g(r)$, Eq. (C5) is obtained.

$$[\nabla\alpha_g\cdot\mathrm{T}]_z = \tau_{rz}\frac{\partial\alpha_g}{\partial r} \tag{C5}$$

The distributions of the interfacial shear stress and void fraction are assumed by Eqs. (C6) and (C7), respectively as:

$$\tau_i \simeq \tau_w\left(\frac{r}{R}\right)^m \tag{C6}$$

$$\frac{\alpha_g}{\alpha_{g0}} = 1 - \left(\frac{r}{R}\right)^n \tag{C7}$$

where τ_i, τ_w, R, m, and n are the interfacial shear stress, wall shear stress, channel radius, exponent, and exponent, respectively.

Substituting Eqs. (C6) and (C7) into Eq. (C5) and integrating Eq. (C5) over a flow channel yields:

$$\langle -[\nabla\alpha_g\cdot\mathrm{T}]_z\rangle = -\langle\nabla\alpha_g\cdot\mathrm{T}_i\rangle_z = -\frac{4\tau_w}{D_H}\langle\alpha_g\rangle C_\tau \tag{C8}$$

where

$$C_\tau = \frac{n+2}{n+(1+m)} \tag{C9}$$

where n is close to unity, resulting in $C_\tau \simeq 1$.

Appendix D

The purpose of Appendix D is to derive Eq. (43).

$$[-\nabla\alpha_g\cdot\mathrm{T}_i]_z = -\tau_{rz}\frac{\partial\alpha_g}{\partial r} \tag{D1}$$

Integrating Eq. (D1) over a flow channel yields:

$$\begin{aligned}\langle[-\nabla\alpha_g\cdot\mathrm{T}_i]_z\rangle &= -\langle\nabla\alpha_g\cdot\mathrm{T}_i\rangle_z = -\frac{1}{A}\int_A \tau_{rz}\frac{\partial\alpha_g}{\partial r}2\pi r dr \\ &= -\frac{1}{A}\lim_{dr\to 0}\tau_{gi}\frac{1-0}{dr}2\pi r_i dr = -\frac{\xi_i}{A}\tau_{gi}\end{aligned} \tag{D2}$$

where ξ_i is the wetted perimeter of the gas core ($=2\pi r_i$). In the derivation of Eq. (D2), it is assumed that the void fraction at the gas-liquid interface changes from 1 to 0. The void fraction is assumed to be uniform in the gas core (=1) and liquid film (=0). A non-zero term in the right-hand side of Eq. (D2) occurs only at the gas-liquid interface.

$$\left\langle \left[-\nabla\alpha_f \cdot \mathrm{T}_i\right]_z \right\rangle = -\langle \nabla\alpha_f \cdot \mathrm{T}_i \rangle_z = -\frac{1}{A}\int_A \tau_{rz}\frac{\partial \alpha_f}{\partial r} 2\pi r dr$$
$$= \frac{1}{A}\lim_{dr\to 0}\tau_{fi}\frac{0-1}{dr}2\pi r_i dr = -\frac{\xi_i}{A}\tau_{fi} = \frac{\xi_i}{A}\tau_{gi} \quad \text{(D3)}$$

It should be noted here that Eq. (D3) is not the same as Eq. (72) in Ishii-Mishima's paper [22] as:

$$\langle [-\nabla\alpha_k \cdot \mathrm{T}_i]_z \rangle = -\frac{\xi_i}{A}\tau_{gi} \quad \text{(D4)}$$

For the gas phase, Eq. (D4) agrees with Eq. (D2), but for the liquid phase, the sign of the right-hand side of Eq. (D3) is positive against negative in Eq. (D4). Substituting Eq. (D4) into Eq. (38) and applying the steady-state condition yield:

$$0 = -\frac{\partial p}{\partial z} - \frac{4}{D_H}\tau_{fw} - \rho_m g_z - 2\frac{\xi_i}{A}\tau_{gi} \quad \text{(D5)}$$

$\langle [-\nabla\alpha_k \cdot \mathrm{T}_i]_z \rangle$ given by Eq. (D4) does not cancel out, resulting in Eq. (D5). Equation (D5) is an incorrect momentum balance under the steady-state conditions.

Appendix E

The purpose of Appendix E is to demonstrate that Eqs. (41) and (42) apply to the mist flow. The gas and liquid (or droplet) momentum equations are given by Eq. (E1) and (E2), respectively.

$$\frac{\partial\langle\alpha_g\rangle\rho_g\langle\langle v_g\rangle\rangle}{\partial t} + \frac{\partial}{\partial z}\langle\alpha_g\rangle\rho_g\langle\langle v_g\rangle\rangle^2 = -\langle\alpha_g\rangle\frac{\partial p_g}{\partial z} - \frac{4}{D_H}\tau_{gw} - \langle\alpha_g\rangle\rho_g g_z + \langle \mathbf{M}_{ig}\rangle_z - \langle\nabla\alpha_g \cdot \mathrm{T}_{gi}\rangle_z \quad \text{(E1)}$$

$$\frac{\partial\langle\alpha_f\rangle\rho_f\langle\langle v_f\rangle\rangle}{\partial t} + \frac{\partial}{\partial z}\langle\alpha_f\rangle\rho_f\langle\langle v_f\rangle\rangle^2 = -\langle\alpha_f\rangle\frac{\partial p_f}{\partial z} - \langle\alpha_f\rangle\rho_f g_z + \langle \mathbf{M}_{if}\rangle_z - \langle\nabla\alpha_f \cdot \mathrm{T}_{fi}\rangle_z \quad \text{(E2)}$$

where $\alpha_{gw} = 1$ and $\alpha_{fw} = 0$ are assumed.

By assuming $\alpha_f = \alpha_f(r)$, Eq. (E3) is obtained.

$$\left[\nabla\alpha_f \cdot \mathrm{T}\right]_z = \tau_{rz}\frac{\partial\alpha_f}{\partial r} \quad \text{(E3)}$$

The distributions of the interfacial shear stress and void fraction are assumed by Eqs. (C6) and (C7), respectively. Substituting Eqs. (C6) and (C7) into Eq. (E3) and integrating Eq. (E3) over a flow channel yields:

$$\left\langle -\left[\nabla\alpha_f \cdot \mathrm{T}\right]_z \right\rangle = -\langle\nabla\alpha_f \cdot \mathrm{T}_i\rangle_z = -\frac{4\tau_w}{D_H}\langle\alpha_f\rangle C_\tau \quad \text{(E4)}$$

Substituting Eq. (E4) with $C_\tau \simeq 1$ into Eq. (E1) and (E2) yields:

$$\frac{\partial\langle\alpha_g\rangle\rho_g\langle\langle v_g\rangle\rangle}{\partial t} + \frac{\partial}{\partial z}\langle\alpha_g\rangle\rho_g\langle\langle v_g\rangle\rangle^2 = -\langle\alpha_g\rangle\frac{\partial p_g}{\partial z} - \langle\alpha_g\rangle\rho_g g_z + \langle \mathbf{M}_{ig}\rangle_z - \langle\alpha_g\rangle F_w \quad \text{(E5)}$$

$$\frac{\partial\langle\alpha_f\rangle\rho_f\langle\langle v_f\rangle\rangle}{\partial t} + \frac{\partial}{\partial z}\langle\alpha_f\rangle\rho_f\langle\langle v_f\rangle\rangle^2 = -\langle\alpha_f\rangle\frac{\partial p_f}{\partial z} - \langle\alpha_f\rangle\rho_f g_z + \langle \mathbf{M}_{if}\rangle_z - \langle\alpha_f\rangle F_w \quad \text{(E6)}$$

which are the same as Eqs. (41) and (42).

References

[1] G.H. Yeoh, Thermal hydraulic considerations of nuclear reactor systems: past, present and future challenges, Exp. Comput. Multiph. Flow 1 (1) (2019) 3–27.
[2] M. Ishii, T. Hibiki, in: "Thermo-Fluid Dynamics of Two-phase Flow, " second ed., Springer, 2011.
[3] M. Klein, S. Ketter, J. Hasslberger, Large eddy simulation of multiphase flows using the volume of fluid method: Part 1 governing equations and a priori analysis, Exp. Comput. Multiph. Flow 1 (2019) 130–144.
[4] C.S.L. Mills, J.P. Schlegel, Interfacial area measurement with new algorithm for grouping bubbles by diameter, Exp. Comput. Multiph. Flow 1 (2019) 61–72.
[5] B. Prakash, H. Parmar, M.T. Shah, V.K. Pareek, L. Anthony, R.P. Utikar, Simultaneous measurements of two phases using an optical probe, Exp. Comput. Multiph. Flow2 1 (2019) 233–241.
[6] Information System Laboratories, "RELAP5/MOD3.3 Code Manual Volume IV: Models and Correlations," NUREG/CR-5535/Rev 1, vol. IV, 2001.
[7] D.R. Liles, et al., TRAC-PF1/MOD1 correlations and models, NUREG/CR-5069 (1988).
[8] U. S. Nuclear Regulatory Committee, "TRACE V5.0 Theory Manual. Field Equations, Solutions Methods, and Physical Models, 2008.
[9] D. Bestion, The physical closure laws in the CATHARE code, Nucl. Eng. Des. 124 (1990) 229–245.
[10] J.J. Jeong, K.S. Ha, B.D. Chung, W.J. Lee, Development of a multi-dimensional thermal-hydraulic system code, MARS 1.3.1, Ann. Nucl. Energy 26 (18) (1999) 1611–1642.
[11] F. Bassenghi, Validation of the CFD Code NEPTUNE for a Full-Scale Simulator for Decay Heat Removal Systems with In-Pool Heat Exchangers, University of Bologna, 2013. Ph. D. Thesis.
[12] S.J. Ha, C.E. Park, K.D. Kim, C.H. Ban, Development of the SPACE code for nuclear power plants, Nucl. Eng. Technol. 43 (2011) 45–62.
[13] D.H. Lee, D.H. Lee, J.J. Jeong, K.D. Kim, On the partition method of frictional pressure drop for dispersed two-phase flows in the RELAP5/MOD3, TRACE V5, and SPACE codes, Nucl. Technol. 198 (1) (2017) 79–84.
[14] B.J. Kim, J. Kim, K.D. Kim, On the wall drag term in the averaged momentum equation for dispersed flows, Nucl. Sci. Eng. 178 (2) (2014) 225–239.
[15] S. Rassame, T. Hibiki, Drift-flux correlation for gas-liquid two-phase flow in a horizontal pipe, Int. J. Heat Fluid Flow 69 (2018) 33–42.
[16] J.G.M. Andersen, K.H. Chu, "BWR Refill-Reflood Program Constitutive Correlations for Shear and Heat Transfer for the BWR Version of TRAC," NUREG/CR-2134, 1983.
[17] C.S. Brooks, T. Hibiki, M. Ishii, Interfacial drag force in one-dimensional two-fluid model, Prog. Nucl. Energy 61 (2012) 57–68.
[18] C.-H. Lin, T. Hibiki, Databases of interfacial area concentration in gas-liquid two-phase flow, Prog. Nucl. Energy 74 (2014) 91–102.
[19] T.-J. Chuang, T. Hibiki, Vertical upward two-phase flow CFD using interfacial area transport equation, Prog. Nucl. Energy 85 (2015) 415–427.
[20] J.D. Talley, T. Worosz, S. Kim, Characterization of horizontal air–water two-phase flow in a round pipe Part II: measurement of local two-phase parameters in bubbly flow, Int. J. Multiphas. Flow 76 (2015) 223–236.
[21] B. Chexal, G. Lellouche, J. Horowitz, J. Healzer, S. Oh, The chexal-lellouche void fraction correlation for generalized applications, NSAC- 139 (1991).
[22] T. Hibiki, M. Ishii, Interfacial area concentration of bubbly flow systems, Chem. Eng. Sci. 57 (18) (2002) 3967–3977.
[23] T. Hibiki, T.H. Lee, J.Y. Lee, M. Ishii, Interfacial area concentration in boiling bubbly flow systems, Chem. Eng. Sci. 61 (24) (2006) 7979–7990.
[24] D. Chisholm, A theoretical basis for the lockhart-martinelli correlation for two-phase flow, Int. J. Heat Mass Tran. 10 (1967) 1767–1778.
[25] R.W. Lockhart, R.C. Martinelli, Proposed correlation of data for isothermal two-phase, two-component flow in pipes, Chem. Eng. Prog. 5 (1949) 39–48.
[26] M. Ishii, N. Zuber, Drag coefficient and relative velocity in bubbly, droplet or particulate flows, AIChE J. 25 (5) (1979) 843–855.
[27] S. Baotong, S. Rassame, S. Nilsuwankosit, T. Hibiki, Drift-flux correlation of oil-water flow in horizontal channels, J. Fluid Eng. 141 (3) (2019) 31301.